Apoptosis (2009) 14:1331–1340
DOI 10.1007/s10495-009-0401-3

ORIGINAL PAPER

Effects of upregulated expression of microRNA-16 on biological properties of culture-activated hepatic stellate cells

Can-Jie Guo · Qin Pan · Bo Jiang · Guang-Yu Chen · Ding-Guo Li

Published online: 26 September 2009

Abstract In our previous studies, we identified miR-16 as being downregulated during activation of hepatic stellate cells (HSCs) by microarray hybridization. However, the roles and related mechanisms of miR-16 in HSCs are not understood. In this study, The miRNA RNAi technique was used to analyze the effects of miR-16 on biological properties of HSCs in vitro. The lentiviral vector encoding miR-16 was constructed and transfected. Furthermore, the expression level of miR-16 was measured by real-time PCR. Cellular growth and proliferation capacity were assayed using the cell counting kit-8 (CCK-8). The apoptosis rate and cell-cycle distribution were measured by flow cytometry. Cell morphological characteristics were identified by phase-contrast microscopy, fluorescence microscopy and electron microscopy. The underlying mechanisms related to the changes in biological properties were assessed. The identity of the recombinant plasmid was confirmed by restriction endonuclease analysis and DNA sequencing. Virus titer was $10^8 >$ ifu/m. Restoring the intracellular miRNAs by miR-16 administration greatly reduced the expression levels of cyclin D1 (CD1). Cell-cycle arrest and typical features of apoptosis were detected in activated HSCs treated with pLV-miR-16. Our results indicate that transduction of miR-16 offers a feasible approach to significantly inhibit HSC proliferation and increase the apoptosis index. Thus, targeted transfer of miR-16 into HSC may be useful for the treatment of hepatic fibrosis.

Keywords Liver fibrosis · Hepatic stellate cells · rno-miR-16 · Lentivirus

Abbreviations

miRNA	microRNA
HSC	Hepatic stellate cell
3′UTR	3′untranslated region
SD	Standard deviation
CCK-8	Cell counting kit-8
CD1	Cyclin D1

Introduction

Hepatic stellate cells (HSCs) have long been considered to be critically important mediators of liver fibrosis [1]. Following liver injury of any etiology, HSCs undergo a response known as "activation," which is the transition of quiescent cells into proliferative, fibrogenic, and contractile myofibroblasts [2]. Several studies recently reported that the number of HSCs are increased associated with its biological properties of HSCs proliferation and counteration of apoptosis, when stimulated by fibrogenic stimuli [3–5]. However, limited understanding of the gene regulation made these characteristics of HSCs still vague and controversial until now.

miRNAs are a recently discovered family of small non-protein-coding RNA about 21–25nt which regulate gene

C.-J. Guo · Q. Pan (✉) · G.-Y. Chen · D.-G. Li (✉)
Digestive Disease Laboratory and Department of Gastroenterology, Xinhua Hospital, School of Medicine, Shanghai Jiaotong University, No. 1665 Kongjiang Road, Shanghai 200092, China
e-mail: lidingguo13612@yahoo.com.cn

Q. Pan
e-mail: pan_qin@yeah.net

B. Jiang
Central South University, Changsha, China

expression at the posttranscriptional level through incomplete or complete complementary binding of miRNAs to target sequences within cellular 3′UTRs [6]. miRNAs have been implicated in a variety of biological processes, including cell proliferation, cell differentiation, apoptosis and so on [7]. In our previous studies, we analyzed the miRNA expression profile in quiescent and in culture-activated primary rat HSCs and identified 21 miRNAs [8]. Meanwhile, bioinformatic analysis revealed the signaling pathways regulated by these miRNAs in HSC activation, we found that apoptosis and cell-cycle pathways appeared to be the most enriched of these differentially downregulated signaling pathways [9].

Using both microarrays and quantitative PCR, we reported previously that nine downregulated miRNAs (miR-341, miR-20b-3p, miR-15b, miR-16, miR-375, miR-122, miR-146a, miR-92b, and miR-126), were identified in rat HSCs during activation. An indispensable role of miRNAs was hypothesized throughout their activation on the basis of signaling pathway alternation. We found miR-16 is most likely to be related with HSCs proliferation, and apoptosis resistance [8, 9]. These data prompted us to validate targets of miR-16 and its related function in liver fibrosis. In our previous studies, we found that miR-16 is involved in regulating apoptosis in activated HSCs by interfering with the expression of Bcl-2, thereby mediating resistance to apoptosis [8]. Here, we performed an overall analysis of the effects of miR-16 on biological properties of HSCs and investigated its related mechanism on the basis of miRNA expression profile and bioinformatic interpretation. These findings may increase our current knowledge about the significance of HSC biological behavior, and provide a novel therapeutic strategy against activation and progression of liver fibrosis.

Materials and methods

Isolation and culture of rat HSC

Primary HSCs were isolated from ten normal male Sprague–Dawley rats (Shanghai Laboratory Animal Center of Chinese Academy of Sciences, weighing 400–500 g) by in situ perfusion and density-gradient centrifugation [10]. The rats received humane care according to the Guide for the Care and Use of Laboratory Animals of the Chinese Academy of Sciences. All materials for HSC isolation were obtained from commercial sources as previously described [11]. After isolation the cells were cultured for 1 day, trypsinized and cultured for 1 additional day, after which time they were harvested as quiescent HSCs. For activated HSCs, HSCs were cultured in uncoated plastic dishes in DMEM supplemented with 10% FBS for total of 14 days. Cell number/viability was determined using the CellometerAutoT4 (Nexcelom Bioscience, Lawrence, MA, USA) based on the trypan blue (Sigma, USA) exclusion method, while their purity was assessed by phase-contrast microscopic appearance and characteristic autofluorescence.

Immunofluorescence staining of rat HSCs

The expression of desmin and CD1 in quiescent (2 days) and culture-activated HSCs (14 days) was evaluated by immunofluorescence staining as previous mentioned [9]. The adherent HSCs were fixed with 4% paraformaldehyde and permeabilized with 0.1% Triton X-100 (Sigma, St Louis, MO, USA). Following blocking in 10% preimmune goat serum for 2 h, cells were incubated with mouse monoclonal anti-desmin (1:100, Santa Cruz, USA) or mouse monoclonal anti-CD1 (1:100, Santa Cruz, USA) overnight at 4°C. Then cells were incubated with TRITIC-conjugated donkey anti-mouse IgG (Sigma; 1:100) or FITC-conjugated goat anti-mouse IgG (1:100, Molecular Probes, USA) for 1 h. Hoechst33258 staining was used to stain the nuclei. TRITIC, FITC and Hoechst33258 fluorescence were visualized using a fluorescence microscope. The positive cells of three randomly selected areas per slide from three slides was used to calculate the expression of CD1 in HSCs.

Lentiviral construction, production and infection

The precursor miR-16 (pre-miR-16) sequences (GenBank accession number NM_000582) were obtained from miRBase (http://microrna.sanger.ac.uk/sequences/). The pre-miR-16 sense and antisense primers were: 5′-ATAGAATTCTTGTATTATTATGTTTGGAC-3′, 5′-ATAGGATCCAAATTATACTAGCAGGA-3′. Lentivector Expression System was purchased from System Biosciences. Packaging and production of lentivirus were performed according to the manufacturer's protocol. Briefly, double-stranded oligonucleotides encoding pre-miR-16 were annealed and inserted into the pCDH-CMV-MCS-EF1-copGFP miRNA expression vector (System Biosciences, SBI). The new miRNA expression vectors (pCDH-CMV-MCS-EF1-copGFP-miR-16) and Lentivirus Package plasmid mix (System Biosciences, SBI) were cotransfected into 293TN cells with Lipofectamine 2000 (Invitrogen). The culture supernatants were collected, concentrated, and used as a virus stock. The viral titer was determined by counting GFP-positive cells after transfection.

Treatment of activated HSCs by miR-16

Activated HSCs were cultured at a density of 2×10^5 ml^{-1} in 25-cm^2 uncoated plastic plates and divided into a normal

group, a negative control group, and miR-16-transfected groups with a multiplicity of infection (MOI) from 10 to 50. At 24 h prior to infection, HSCs were plated in each well of 6-well plates, then infected with recombinant viruses (pLV-miR-16 or pLV-GFP) at a different multiplicity of infection (MOI) of for 6 h at 37°C, followed by the addition of fresh growth medium. Three days later, all lentiviral vectors expressed enhanced green fluorescent protein (GFP), which allowed for titering and measuring their infection efficiency in transfected cells.

For cell survival and apoptosis, cells were stained with annexin V-FITC and propidium iodide (PI) according to the manufacturer's protocol (Bender MedSystems, Vienna, Austria), and subjected to flow cytometry 72 h after infection. The stained cells were divided into three groups: cells in the V^-/PI^- subgroup survived with an intact membrane; cells in the V^+/PI^- subgroup were apoptotic with an intact membrane and phosphatidylserine translocation; cells in the V^+/PI^+ subgroup were necrotic with an impaired membrane and phosphatidylserine translocation. All experiments were performed in triplicate.

Quantitative RT-PCR analysis of CD1 and miR-16 expression

Total RNA was isolated using Trizol reagent according to the manufacturer's instructions. RNA purity and concentration were determined by electrophoresis and a BioPhotometer (Eppendorf AG, Hamburg, Germany).The extracted total RNA of HSCs from the three groups was reverse transcribed into cDNA using ExScript™ RT reagent Kit (TAKARA, Kusatsu, Japan). Expression of these mature miRNAs was assayed using stem-loop RT followed by PCR analysis, as previously described [12]. PCR analysis was performed in triplicate for each sample. The relative amount of miRNA was normalized against U6 snRNA or GAPDH, and the fold change was calculated by the 2-[delta][delta] Ct method [13].The sense and antisense primers used in this study were: miR-16 (MIMAT0000785, 64 bp); GSP 5′-GGGGTAGCAGCACGTAAATA-3′, 5′-GT GCGTGTCGTGGAGTCG-3′; U6 (K00784, 89 bp) 5′-GCT TCGGCAGCACATATACTAAAAT-3′, 5′-CGCTTCACGA ATTTGCGTGTCAT-3′; CD1 (NM_171992, 358 bp) 5′-CA GCCCACTCAACATCA-3′, 5′-ATCCCTCCGACTTTGC-3′; GAPDH:(NM-002046, 450 bp) 5′-ACCACAGTCCATG CCATCAC-3′, 5′-TCCACCACCCTGTTGCTGTA-3′.

Detection of CD1 by Western-blot analysis

Total proteins were prepared by standard procedures and quantified by the BCA method (Pierce, Rockford, USA). Thirty micrograms of protein per sample were loaded onto a 10% SDS-polyacrylamide gel. After electrophoresis, the protein was transferred onto a PVDF membrane (Millipore, Billerica, MA, USA) by electro-elution. The membrane was incubated with anti-CD1 antibody (1:500; Santa Cruz, CA, USA) overnight at 4°C and with HRP-conjugated goat anti-mouse IgG (1:5000; Jackson ImmunoResearch) for 2 h at room temperature. After washing, the membrane was processed using SuperSignal West Pico chemiluminescent substrate (Pierce, Rockford, IL, USA) and anti-actin antibody (Santa Cruz, CA, USA) (1:500) as an internal standard.

In vitro proliferation assay

Cells were seeded in 96-well plates and cultured for 24 h. Cells were starved for 24 h by replacing the media with serum-free media, followed by infection with recombinant viruses (pLV-miR-16 or pLV-GFP) at a MOI 50. Cell culture was continued for 24, 48 and 72 hours and assessed using the Cell Counting Kit 8 (Dojindo, Kumamoto, Japan). The absorbance value of each well was determined at 450 nm using a microplate reader (Molecular Devices, Tokyo, Japan).

Cell-cycle analysis

Cells were transfected with pLV-miR-16. At 72 hours after transfection, floating and adherent cells were harvested, combined, and processed. Alternatively, nocodazole (100 ng/ml; Sigma–Aldrich) was added and cells were further incubated for 16–20 h before harvesting. The supernatant from each well was combined with cells harvested from each well by trypsinization. Cells were collected by centrifugation, fixed with ice-cold 70% ethanol, washed with phosphate-buffered saline (PBS), and resuspended in 0.5 ml of PBS containing propidium iodide (500 μg/ml) and RNase A (1 mg/ml). After a final incubation at 37°C for 30 min, cells were analyzed using a FACSCalibur flow cytometer (Becton–Dickinson). A total of 10,000 events were counted for each sample. Data were analyzed using FlowJo software (Tree Star, Ashland, OR).

Hoechst 33258 staining for HSCs

Cells were incubated with or without miR-16 or miR-15b, harvested, fixed with 4% paraformaldehyde for 30 min at 25°C, washed three times with ice-cold PBS, and exposed to 10 mg/l Hoechst 33258 (Beyotime Institute of Biotechnology, Jiangsu, China) in the dark at room temperature for 10 min. Stained cells were observed using a fluorescence microscope. The cells with condensed chromatin and shrunken nuclei were classed as apoptotic.

Apoptosis examined by transmission electron microscopy

HSCs were infected (MOI 50) in six-well plates 72 h after plating with indicated lentivirus in DMEM (5% FCS). Three days later, the medium was replaced (10% FCS) and cells were fixed in 3% glutaraldehyde/0.1 M phosphate buffer (pH 7.4) for 15 min after incubation for 24–48 h. Scraped cells were centrifuged for 10 min at low speed and the cell pellet was mixed with 3% agarose at 50°C by addition of 3% glutaraldehyde. Blocks of embedded cells were washed with PBS and osmification was performed with 1% osmium-tetraoxide in phosphate buffer for 1 h. Cells were then dehydrated with standard alcohol series, infiltrated in a mixture of epoxy resin/propylene oxide (1:1) for 30 min and flat-embedded in pure epoxy resin for 60 min using dried, labeled silicon moulds. Sections (1 mm) were counterstained with Toluidine Blue, and ultrathin sections (80–100 nm) were prepared using a diamond knife and mounted on copper grids. The grids were stained with uranyl acetate and lead citrate, air-dried and examined using a Philips transmission electron microscope TEM 400 at 60 kV.

Statistical analysis

All the results are expressed as mean ± standard deviation (SD). Statistical analysis was performed using the Student's *t*-test for comparison of two groups, and ANOVA for multiple comparisons. In both cases, differences of $P < 0.05$ were considered statistically significant.

Results

Expression levels of CD1 in HSCs derived from normal S-D rats

About 5×10^8 ml^{-1} HSCs were harvested from each rat. The percentage of freshly isolated living HSCs was up to 95% as defined by trypan blue staining; cells maintained a small and round appearance with quiescent phenotype at 48 h. After stimulation with a 327-nm laser, up to 95% HSCs showed a blue-green intrinsic autofluorescence due to vitamin-A-rich droplets. More than 95% of the HSCs showed positive desmin staining at day 2 and day 14, indicating high purity of HSCs. Immunofluorescence staining analysis showed markedly increased levels of CD1 in activated HSCs compared with quiescent HSCs ($P < 0.05$) (Fig. 1, 2).

Lentiviral delivery of miR-16

Recombinant lentivirus is the most widely used vectors to deliver genes to HSCs and is associated with high transduction efficiencies for stable integration and long-term

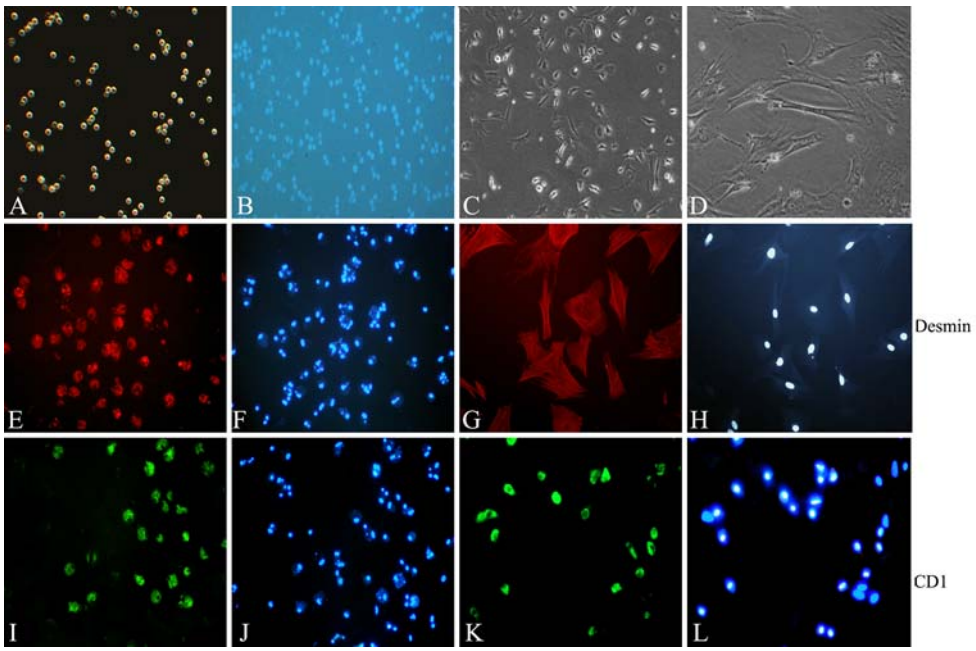

Fig. 1 Characterization of HSCs isolated from rat liver (magnification ×200). **a** Cell morphology of isolated cultured HSCs. **b** Spontaneous fluorescence of cultured HSCs after 24 h. **c**, **d** After isolation, the cells were cultured for 2 days (quiescent HSCs) or for 14 days (activated HSCs). **e**, **i** Immunofluorescence analysis of desmin and CD1 expression in quiescent HSCs. **g**, **k** Desmin and CD1 expression in activated HSCs. Hoechst 33258 nuclear staining for all conditions is shown in panels **f**, **h**, **j**, and **l**

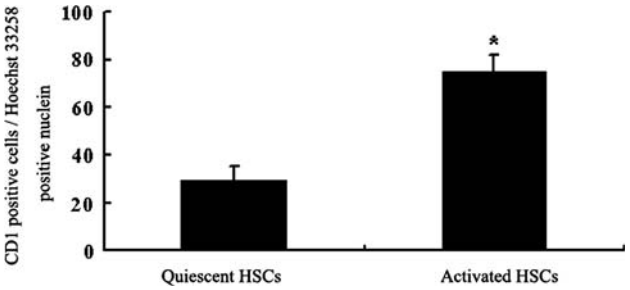

Fig. 2 Immunofluorescence staining assay for CD1 in HSCs. * Statistically significant differences. $P < 0.05$ versus quiescent group

expression of the transgene; it is also a favorable vector in mammalian cells. The lentivectors produced by System Biosciences (SBI) are third-generation lentivectors developed for gene-therapy applications. The schematic in Fig. 2 outlines the general steps required for packaging of HIV-based expression constructs and transduction and expression of the viral expression construct in target cells. The recombinant plasmid (pCDH-CMV-MCS-EF1-copGFP-miR-16) was confirmed by restriction endonuclease analysis and DNA sequencing. Virus titer was $10^8 >$ ifu/ml. The efficiency of transfection was estimated by determining the percentage of green fluorescence protein (GFP)-positive cells and the results of FACS analysis confirmed that 99% HSCs were transduced with pLV-miR-16 (MOI: 50) (Fig. 3a).

To confirm cell viability and apoptosis at the single-cell level, we used the annexin-V/PI assay. Results showed that, 72 h after lentivirus-infection, the pLV-miR-16 transduction efficiency at MOI of 50 was nearly 65.6% with good cell viability and less than 4% cell mortality in each group. Significantly more apoptotic cells were found in the miR-16-transfected cells when MOI was 50, but there were no differences in the level of necrosis between pLV-miR-16 (MOI:50) and the control-transfected group. Therefore, we considered that MOI of 50 was effective. miR-16-treated HSCs induced apoptosis of HSCs but displayed no further damage to cell viability (Fig. 3b). The subsequent assays were performed using pLV-mediated gene transfer at MOI of 50.

miR-16 downregulated CD1 at the posttranscriptional level

Examination of the homology between miR-16 and CD1 mRNA sequences showed that the eight nucleotides in the seed region of miR-16 were complementary to bases 3360–3367 of the CD1 3′UTR (NM_171992).Thus, an inhibitory effect of miR-16 on CD1 was inferred. To further investigate the actions of miR-16 on CD1, the expression of CD1 was investigated at the mRNA and protein levels. Both RT-PCR, immunofluorescence staining analysis and western blot exhibited markedly increased levels of CD1 in activated HSCs compared with those in quiescent HSCs ($P < 0.05$). After being transfected with pLV-miR-16 at a MOI of 50 for 72 h, the expression of miR-16 increased significantly, whereas the protein levels of CD1 were downregulated significantly compared with control ($P < 0.05$) (Fig. 4). This finding indicates that CD1 is regulated by miR-16 in HSCs.

miR-16 inhibits HSCs proliferation

To verify whether the miR-16 family triggered G1 arrest by regulating the expression of CD1 in HSCs, we assessed cell proliferation using the CCK-8 assay. Figure 5 showed that inhibition of CD1 expression by RNAi suppressed growth of HSCs cells. Cell-cycle analysis showed that cell cultures transfected with miR-16 had increased numbers of cells in G0/G1 phase (diploid DNA content) and corresponding decreases in the numbers of cells in S and G2/M phase. These results indicate that miR-16 contributes to induction of G1 arrest in HSCs, at least partially through downregulation of CD1 (Fig. 5).

Morphology changes in HSCs

Morphology changes in HSCs demonstrated that knockdown of Bcl-2 expression by miR-16 induces HSCs cells to undergo apoptotic cell death. At 3 days after infection with miR-16, HSCs showed nuclear blebbing and cellular disintegration, all of which are characteristic of apoptosis. To further characterize these changes, we performed Hoechst 33258 nucleic acid staining and electron microscopic analysis. Typical apoptotic morphological changes such as condensed chromatin and shrunken crimpled and condensed gray-blue nuclei were found in the miR-16-treated HSCs by fluorescence microscopy analysis. HSCs infected with control viruses showed the usual ultrastructural morphology and their nucleus was euchromatic and acentric with several prominent nucleoli (Fig. 6). By contrast, after infection with miR-16 the chromatin arrangements in the nuclei markedly changed (Fig. 6). Nuclear heterochromatin condensation and fragmentation, typical features of apoptosis, were noted. In later stages of apoptosis, nuclear blebbing and shrinkage were observed and nuclei were typically surrounded by highly condensed cytoplasm. Again, these results show that the introduction of miR-16 into HSCs induces the mitochondrial-dependent apoptosis pathway.

Discussion

The miR-16 (miRNA-16) family is known to be associated with cell proliferation and apoptosis regulation, and has

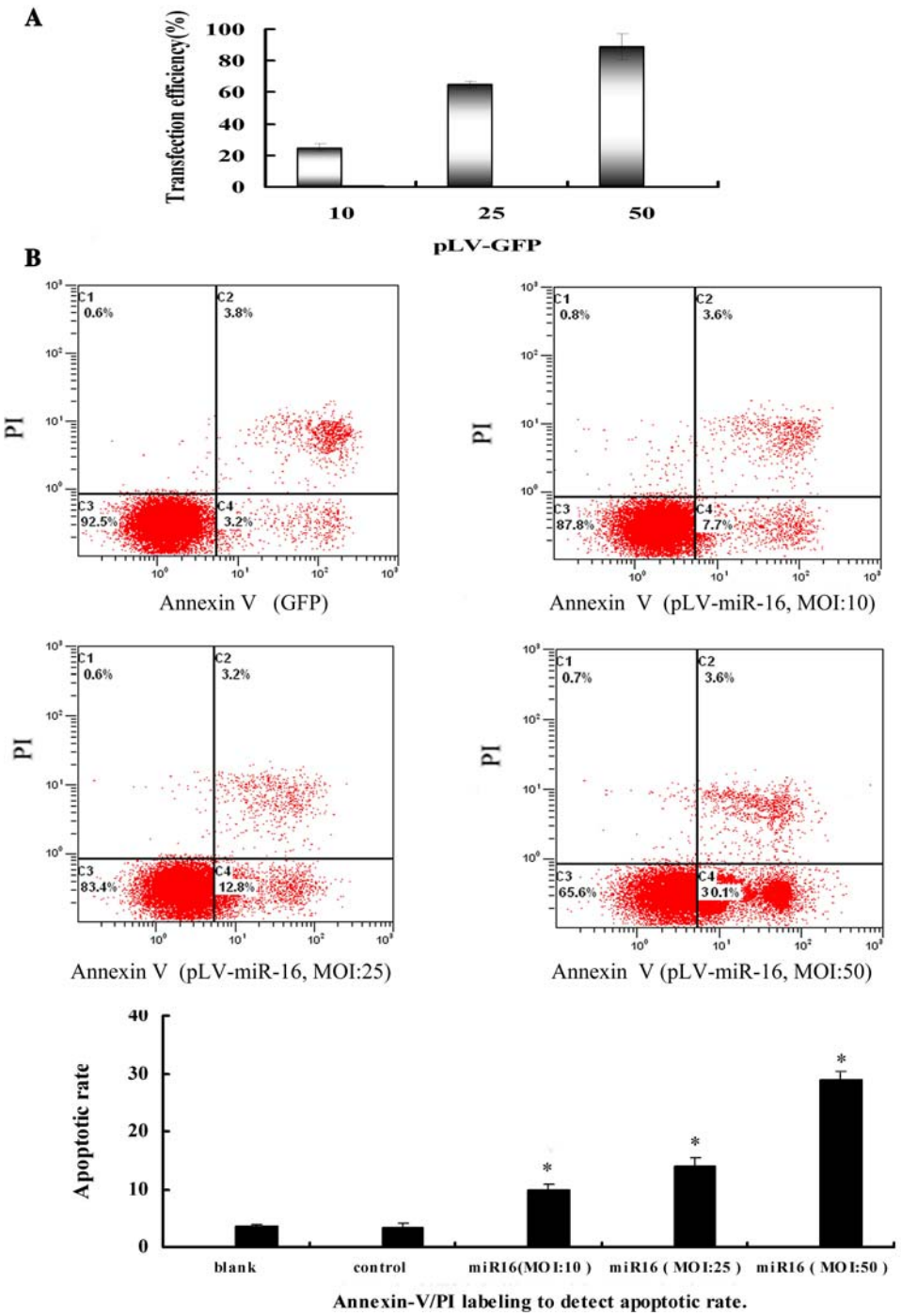

Fig. 3 Titer determination for pLV-GFP in HSCs. **a** Three different multiplicities of infection (MOIs; 10, 25 and 50) were tested in a 6-h transduction experiment in serum-free media. The efficiency of transduction was estimated by determining the percentage of green fluorescence protein (GFP)-positive cells. **b** Flow cytometry analysis of HSC viability and apoptosis at 72 h after infection. Only the annexin V^+/PI^- cells (shown as C4 area) were classed as apoptotic cells and counted. * Indicates significant differences. $P < 0.05$ vs. control group

been extensively analyzed in tumor cell lines [14]. miR-16 is located on chromosome 13q14, where a deletion has been reported in more than 60% of B-cell chronic lymphoid leukaemia (B-CLL) patients [15]. miR-16 has been shown to be implicated in the induction of apoptosis by targeting Bcl-2 and involved in cell-cycle regulation in several diseases, such as CLL, pituitary adenomas, and prostate carcinoma, by regulating multiple cell-cycle genes including CCND1 (cyclin D1), CDK6 (cyclin-dependent kinase 6), CDC27 (cell-division cycle 27), CARD10 (caspase recruitment domain 10), C10orf46 (chromosome10 open-reading frame 46) and CDC2 (cell division cycle 2) [16–19]. These genes have all been shown to be biological targets of miR-16. Among these target genes, Bcl-2 and CD1 within the our previous miRNA-gene networks, which had the highest ratio and enrichment in the apoptosis-related pathway and cell cycle pathway, respectively, were noted [9]. CD-1, which can be rarely detected in the normal

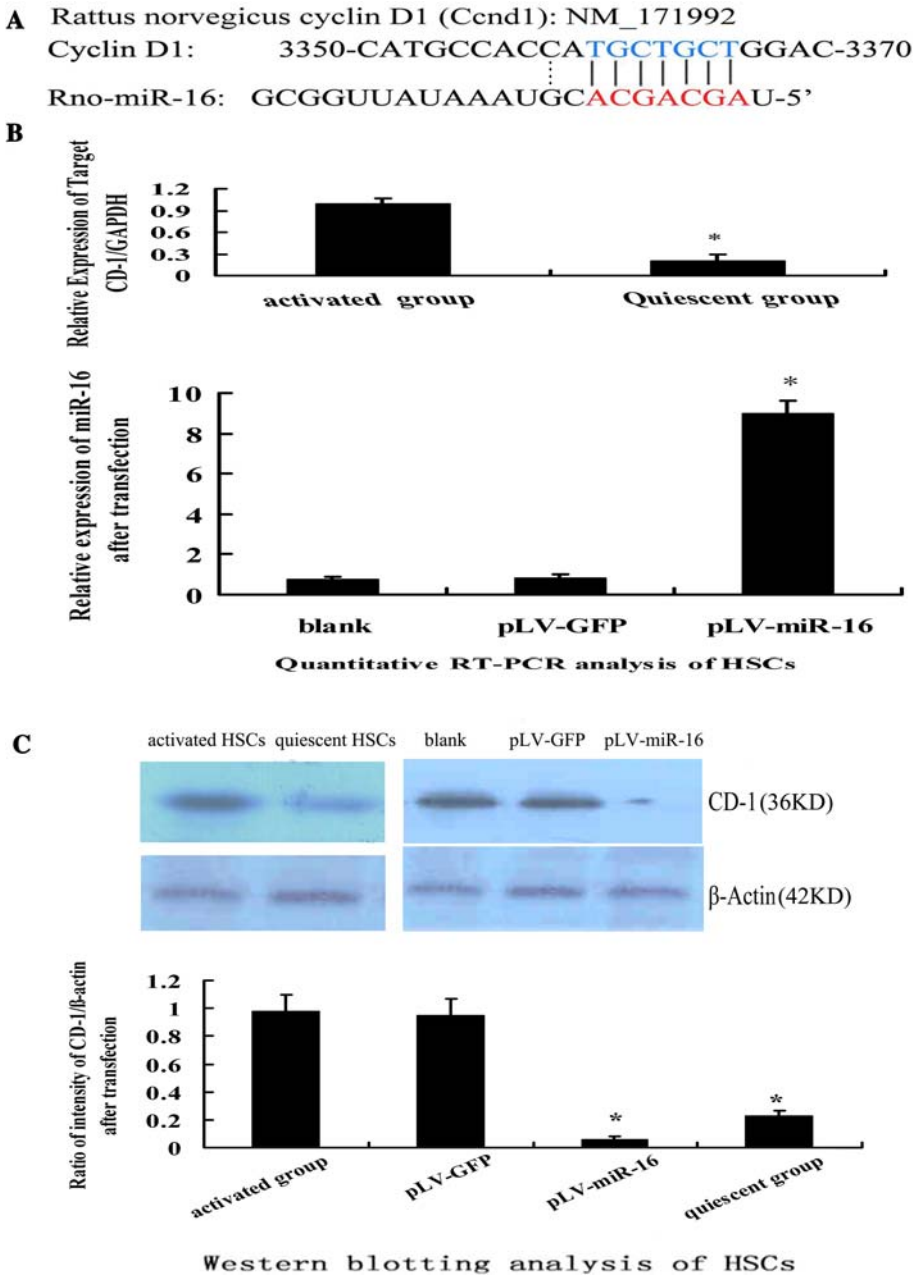

Fig. 4 CD1 is a target of miR-16. **a** Putative binding sites of miR-16 in the CD1 3′UTR. **b** Top: The mRNA levels of CD1 in quiescent and activated HSCs detected by RT-PCR. Bottom: miR-16 mRNA level were assessed at 72 h after transfected with pLV-miR-16. **c** CD1 protein level was assessed at 72 h after transfection of miR-16. * Indicates significant differences. $P < 0.05$ vs. activated group

HSCs and non-proliferative senescent HSCs, is overexpressed in culture-activated HSCs and intra-hepatic HSCs after DMN(dimethylnitrosamine) injury [20, 21]. Recent studies have partially attributed the proliferation of activated HSCs to the over-expression of CD-1 [20, 22]. Furthermore, Using bioinformatics tools, we found that miR-16 was the only miRNA targeting CD-1 with 8 complementary nucleotides. Moreover, the levels of miR-16 were inversely correlated with that of CD-1 in both quiescent and activated HSCs, which was also in agreement with earlier studies in other tumor lines [23]. Taken together, miR-16 are likely to play important roles in the proliferation of HSCs by targeting CD-1.

Our experimental findings were consistent with these predictions. CD1 has a critical role in maintaining the integrity of the G1/S checkpoint, and is often detected at the protein and mRNA levels in activated rather than quiescent HSCs in our experiments by immunofluorescence analysis, QRT-PCR analysis and western blot. moreover, transfection of pLV-miR-16 greatly reduced the expression level of CD1. A combination of CCK8 and flow cytometry also demonstrated marked cell arrest in miR-16-treated activated HSCs. This result provides the first evidence that restoration of the level of miR-16 induces G1 arrest in HSCs with a myofibroblast-like phenotype, partially by regulating CD1. Together with results from other laboratories, miR-16 is

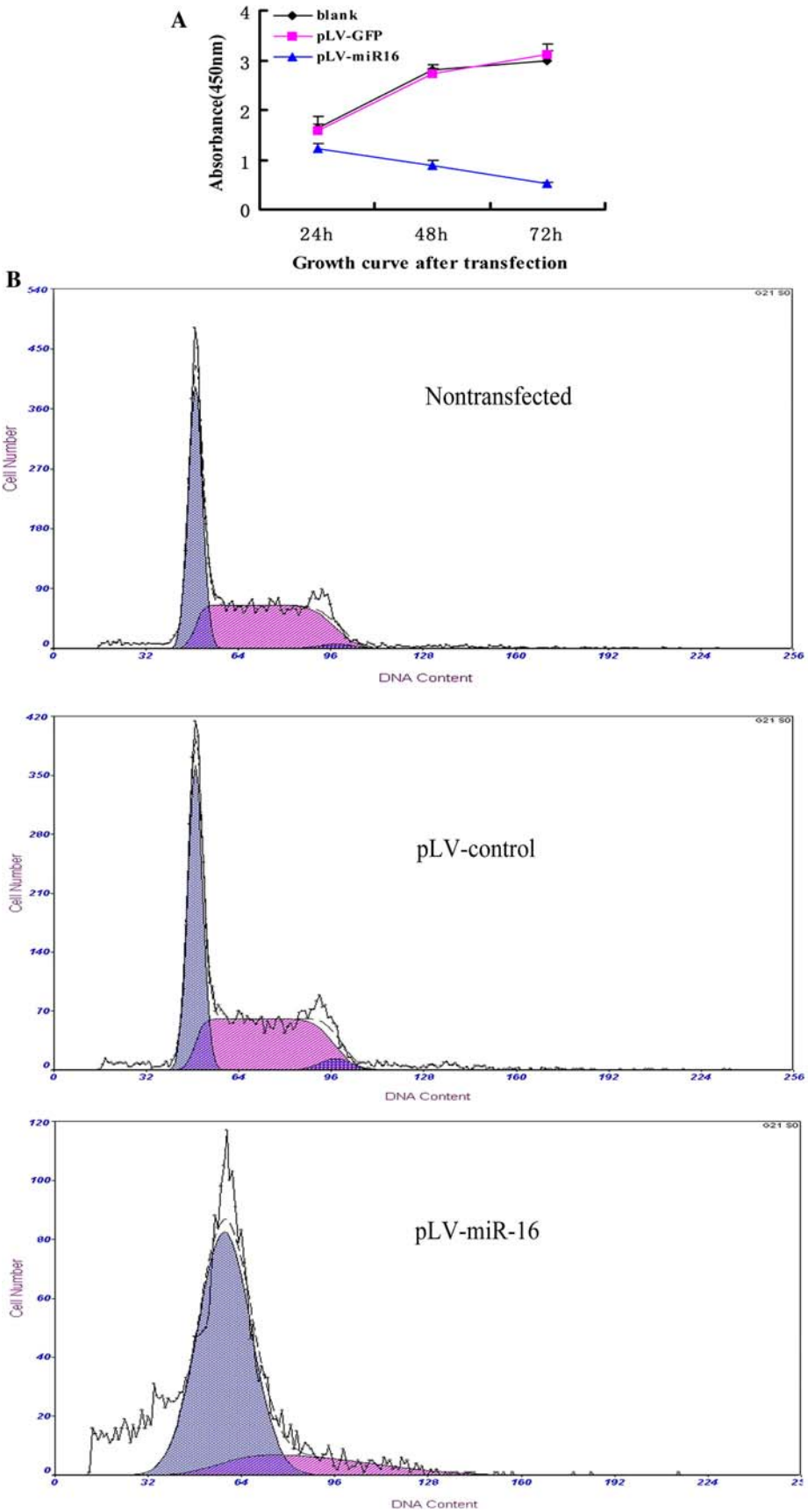

Fig. 5 Knockdown of CD1 expression by miR-16 suppressed proliferation and induced G1 arrest in HSCs. **a** The proliferation curve of HSCs. Cell proliferation was analyzed using CCK-8 cell proliferation assay kits. Each value represents the mean of six replicates. The proliferation of HSCs transfected with pLV-miR-16 was suppressed significantly compared with cells that were not transfected or were transfected with control vector. **b** HSC cell cycle was analyzed by FACS; untransfected group (G1 41.802%, S 54.005%, G2/M 4.193%); control group (G1 42.834%, S 53.655%, G2/M 3.511%); pLV-miR-16 group (G1 82.182%, S 17.818%, G2/M 0%). Knockdown of CD1 expression induced G1 arrest in HSCs

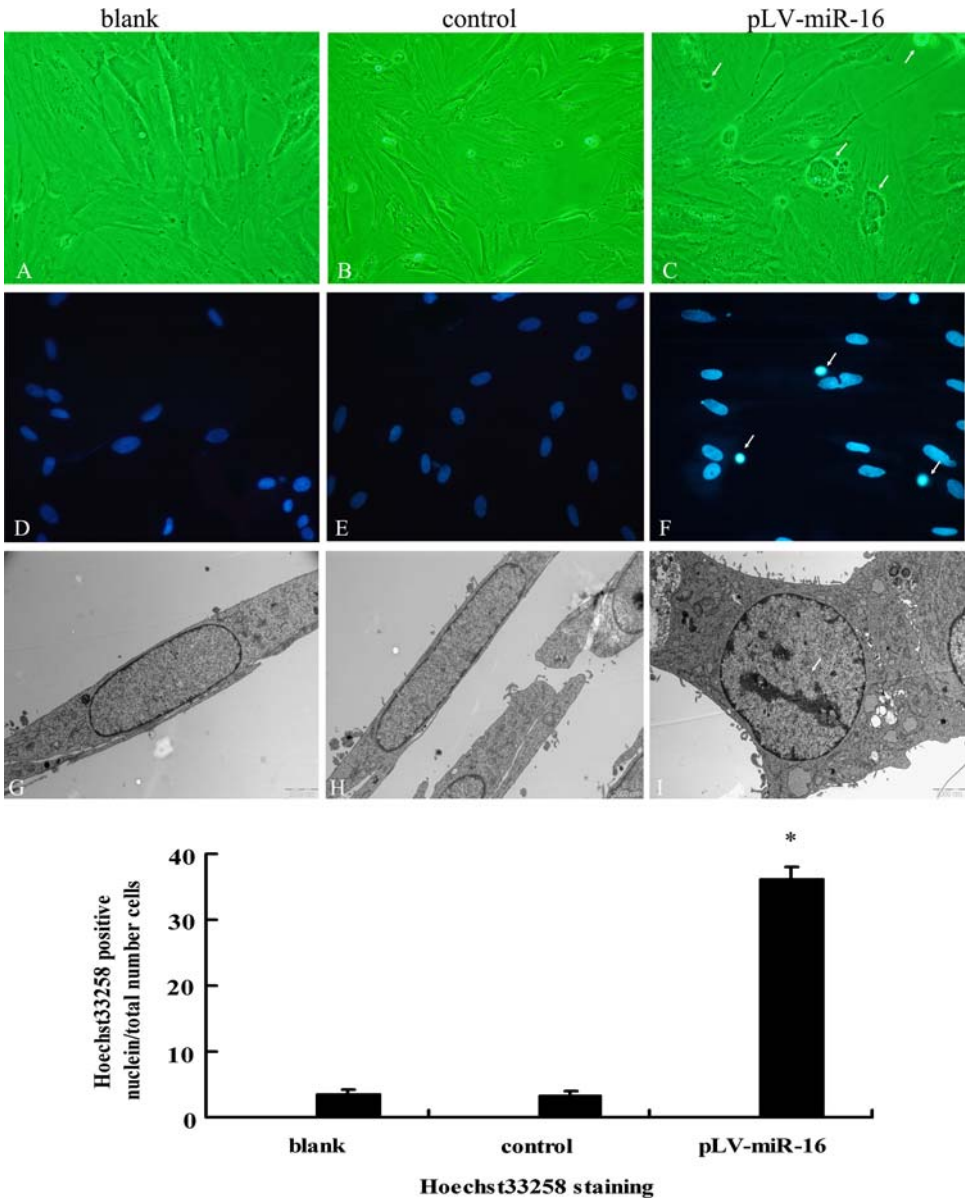

Fig. 6 The effects of miR-16 on apoptosis of activated HSCs. Light microscopy analysis of HSCs (magnification ×400). **a** Blank (without miRNA); **b** pLV-GFP; **c** pLV-miR-16. Fluorescent images of HSCs using Hoechst 33258 staining (×400). **d** blank (without miRNA); **e** pLV-GFP; **f** pLV-miR-16. Electron microscopy analysis (×7400): Phenotypic appearance of nuclei from uninfected HSCs (**g**), HSCs infected with pLV-GFP (**h**), or pLV-miR-16 (**i**). Apoptosis ends in cytoplasmatic disintegration with nuclear blebbing and shrinkage, and condensed nuclei (white arrow). These changes were not seen in uninfected HSC or in cells infected with pLV-GFP. * Indicates significant differences. $P < 0.05$ vs. control group

involved in cell cycle progression and cellular proliferation by regulating multiple proteins. Moreover, G1 arrest is a multi-protein regulated process and one miRNA could target multiple genes, therefore, it remains unclear whether there are other G1/S transition genes regulated by miR-16 or other miRNAs.

In our previous study, Bcl-2 was shown to be an anti-apoptotic protein and identified as having an important role in preservation of mitochondrial integrity and protection of cells from apoptotic cell death. A specialized analysis further revealed that restoring the intracellular miRNA levels by administration of miR-16 greatly reduced the level of Bcl-2, and increased the expression levels of caspases 3, 8, and 9. In this study, miR-16 mediated by lentiviral vectors—which could induce a long-lasting downregulation in gene expression—was used to analyze the pro-apoptotic effects on HSCs. We found evidence that apoptosis follows transfection with miR-16. Flow-cytometry analysis showed that the apoptosis rate of cells treated with miR-16 was significantly higher than those of untreated HSCs and control cells. To investigate the effects of miR-16 on morphological changes of HSCs, the most evident pro-apoptosis effect was observed in the miR-16-treated group by Hoechst33258 staining and transmission electron microscopy analysis. These results showed that restoring the intracellular miRNA levels by miR-16 significantly promoted HSCs apoptosis, which is in agreement with the results of our previous studies.

Increasing evidence indicates that miR-16 targets genes that are involved in cell biological processes other than

CD1-induced cell-cycle arrest and Bcl-2-induced apoptosis. Indeed, there are other signaling pathways and related target genes relevant to miR-16, such as the Wnt3a and CDK6-mediated pathways [18, 24]. Nevertheless, critical members of Wnt3a and CDK6 signaling pathways were not found in the miRNA gene networks. However, it is likely that miR-16 may target other genes that are relevant to the biological changes in HSCs.

In conclusion, our results show that miR-16 negatively regulates CD1 as well as Bcl-2 expression, and promotes G1 arrest and HSC apoptosis. The results support the hypothesis that targeting miRNAs is superior to use of antisense mRNAs and RNAi to study gene functions, and possibly also in gene therapy [25]. Monitoring miR-16 levels in liver fibrosis may thus facilitate better disease diagnosis and therapy.

Acknowledgements This work is supported by the Foundation of Shanghai Commission of Science Technology of Research Program (O7JC14044).

References

1. Sprenger H, Kaufmann A, Garn H, Lahme B, Gemsa D, Gressner AM (1997) Induction of neutrophil-attracting chemokines in transforming rat hepatic stellate cells. Gastroenterology 113:277–285
2. Kruglov EA, Correa PR, Arora G, Yu J, Nathanson MH, Dranoff JA (2007) Molecular basis for calcium signaling in hepatic stellate cells. Am J Physiol Gastrointest Liver Physiol 292:G975–G982
3. Novo E, Marra F, Zamara E, Valfrè di Bonzo L, Monitillo L, Cannito S et al (2006) Overexpression of Bcl-2 by activated-humanhepatic stellate cells: resistance to apoptosis as a mechanism of progressive hepatic fibrogenesis in humans. Gut 55: 1174–1182
4. Kawada N (2006) Human hepatic stellate cells are resistant to apoptosis: implications for human fibrogenic liver disease. Gut 55: 1073–1074
5. Lin YL, Lee TF, Huang YJ, Huang YT (2006) Antiproliferative effect of salvianolic acid A on rat hepatic stellate cells. J Pharm Pharmacol 58:933–939
6. Chitwood DH, Timmermans MC (2007) Target mimics modulate miRNAs. Nat Genet 39:935–936
7. Ambros V (2004) The functions of animal miRNA. Nature 431: 350–355
8. Guo CJ, Pan Q, Li DG, Sun H, Liu BW (2009) miR-15b and miR-16 are implicated in activation of the rat hepatic stellate cell: an essential role for apoptosis. J Hepatol 50:766–778
9. Guo CJ, Pan Q, Cheng T, Jiang B, Chen GY, Li DG (2009) Changes in microRNAs associated with hepatic stellate cell activation status identify signaling pathways. FEBS J 276:5163–5176
10. Friedman SL, Roll FJ (1987) Isolation and culture of hepatic lipocytes, Kupffer cells, and sinusoidal endothelial cells by density gradient centrifugation with Stractan. Anal Biochem 161: 207–218
11. Ying-Bin Hu, Ding-Guo Li, Han-Ming Lu (2007) Modified synthetic siRNA targeting tissue inhibitor of metalloproteinase-2 inhibits hepatic fibrogenesis in rats. J Gene Med 9:217–229
12. Chen C, Ridzon DA, Broomer AJ, Zhou Z, Lee DH, Nguyen JT et al (2005) Real-time quantification of microRNAs by stem-loop RTPCR. Nucleic Acids Res 33:e179
13. Livak KJ, Schmittgen TD (2001) Analysis of relative gene expression data using real-time quantitative PCR and the 2(-Delta Delta C(T)) method. Methods 25:402–408
14. Mraz M, Pospisilova S, Malinova K, Slapak I, Mayer J (2009) MicroRNAs in chronic lymphocytic leukemia pathogenesis and disease subtypes. Leuk Lymphoma 50:506–509
15. Raveche ES, Salerno E, Scaglione BJ et al (2007) Abnormal microRNA-16 locus with synteny to human 13q14 linked to CLL in NZB mice. Blood 109:5079–5086
16. Bottoni A, Piccin D, Tagliati F, Luchin A, Zatelli MC, degli Uberti EC (2005) miR-15a and miR-16-1 down-regulation in pituitary adenomas. J Cell Physiol 204:280–285
17. Bandi N, Zbinden S, Gugger M et al (2009) miR-15a and miR-16 are implicated in cell cycle regulation in a Rb-dependent manner and are frequently deleted or down-regulated in non-small cell lung cancer. Cancer Res 69:5553–5559
18. Bonci D, Coppola V, Musumeci M et al (2008) The miR-15a-miR-16-1 cluster controls prostate cancer by targeting multiple oncogenic activities. Nat Med 14:1271–1277
19. Linsley PS, Schelter J, Burchard J et al (2007) Transcripts targeted by the microRNA-16 family cooperatively regulate cell cycle progression. Mol Cell Biol 27:2240–2252
20. Kim MR, Kim HS, Lee MS, Lee MJ, Jang JJ (2005) Cell cycle protein profile of the hepatic stellate cells (HSCs) in dimethylnitrosamine-induced rat hepatic fibrosis. Exp Mol Med 37:335–342
21. Dudas J, Saile B, El-Armouche H, Aprigliano I, Ramadori G (2003) Endoreplication and polyploidy in primary culture of rat hepatic stellate cells. Cell Tissue Res 313:301–311
22. Chen MH, Chen SH, Wang QF et al (2008) The molecular mechanism of gypenosides-induced G1 growth arrest of rat hepatic stellate cells. J Ethnopharmacol 117:309–317
23. Chen RW, Bemis LT, Amato CM et al (2008) Truncation in CCND1 mRNA alters miR-16-1 regulation in mantle cell lymphoma. Blood 112:822–829
24. Liu Q, Fu H, Sun F et al (2008) miR-16 family induces cell cycle arrest by regulating multiple cell cycle genes. Nucleic Acids Res 36:5391–5404
25. Stenvang J, Kauppinen S (2008) MicroRNAs as targets for antisense-based therapeutics. Expert Opin Biol Ther 8:59–81